EAST EUROPEAN JOURNAL OF PHYSICS. 1. 294-307 (2024)
DOI:10.26565/2312-4334-2024-1-26 ISSN 2312-4334

DFT STUDIES ON ELECTRONIC, ELASTIC, THERMOELECTRIC AND OPTICAL PROPERTIES OF NEW HALF-HEUSLER XRhZ (X =V, Nb AND Z = Si, Ge) SEMICONDUCTORS

Bendehiba Sid Ahmed[a], Besbes Anissa[a], Djelti Radouan[a]*, Najwa Al Bouzieh[b], I. Kars Durukan[c] Noureddine Amrane[b]

[a] Technology and Solids Properties Laboratory, University of Mostaganem (UMAB), Algeria
[b] Physics Department, College of Science, United Arab Emirates University (UAEU), 15551, Al Ain, UAE
[c] Department of Physics, Faculty of Science, Gazi University, 06500 Ankara, Turkey
**Corresponding Author e-mail: Radouane.djelti@univ-mosta.dz, djeltired@yahoo.fr*
Received November 12, 2023; revised December 8, 2023; accepted December 20, 2023

Density functional theory is used to explore the physical properties of the new half-Heusler alloys XRhZ (X =V, Nb and Z = Si, Ge). The exchange-correlation effects were treated by the TB-mBJ potential. The four studied compounds are nonmagnetic semiconductor with an indirect band gap. The formation enthalpy, cohesive energy and phonon band structures demonstrated that these semiconductors are structurally and dynamically stable. It was predicted by the elastic study that the XRhZ compounds (X = V, Nb and Z = Si, Ge) have stable mechanical properties, they possess an anisotropic character and reveal the ductile nature with a B/G ratio >1.75. The optical results show an interesting photocatalytic potential for the NbRhSi and NbRhGe semiconductors, they exhibit a high absorption coefficient in the visible domain, which is around 112.10^4 cm^{-1}. For energies greater than 10 eV (UV domain), the refractive index is less than one. The thermoelectric results confirmed that the XRhZ (X=V, Nb and Z=Si, Ge) compounds are very attractive for thermoelectric devices working in large temperature range including ambient temperature.
Keywords: *Half-Heusler alloys; Semiconductor; Elastic properties; Seebeck coefficient; Merit factor; Absorption coefficient; Reflectivity*
PACS: 71.20.-b, 72.15.Jf, 72.25.Ba, 73.50.L, 52.70.Kz

1. INTRODUCTION

Half-Heusler (HH) alloys have involved a remarkable interest over the past years due to their several properties in various technological domains, such as magnetic, optical, thermoelectric, piezoelectric, superconducting and topological properties **[1-8]**. The valence electron count (VEC) has always been found as responsible of the most physical and thermo-electrical properties **[9-10]**. The HH compounds with VEC of 18 are nonmagnetic semiconductors with fascinating optoelectronic properties due to their tunable band gap over broad energy range **[11-12]**. In addition, their smaller bandgap and high electrical conductivity and Seebeck coefficient make them effective in thermoelectric applications **[13-14]**. This type of material is composed by an X^{+n} ion occupying in a zinc blende YZ^{-n} sub-lattice and where the VEC linked with the YZ^{-n} sub-lattice is 18 ($d^{10}s^2p^6$) **[15-16]**. The valence electrons of the X atom are transferred to the Y and Z atoms, which are more electronegative, and thus acquire a closed shell configuration ($s^2p^6d^{10}$). P.K. Kamlesh et al., **[17]** explored by ab-initio calculations the optical possessions of AlNiX (X = P, As and Sb) HH, they confirm that the AlNiP and AlNiAs compounds are well suited for use as shields against high-energy of UV radiation due to their large reflectivity values in this area. Y.Wang et al., **[18]** give a theoretical analysis of transport properties of NbXGe (X = Rh, Ir) H.H materials, subject to network constraints. They have found that for a strain of −6%, the ZT value of NbRhGe has doubled by 50% compared with the unstrained case, so, they state that these materials are promising candidates for TE applications. D.M. Hoat **[19]** has investigated a series of HH compounds based on tantalum and having a VEC of 18, he noted that all the materials studied are indirect band gap semiconductor. The difference between the band gap values is due to the degree of overlap that exists between the Ta-5d and X-4d orbitals. Furthermore, the denser electronic states, close to the Fermi level (**E_F**), of TaRhSn and TaRhPb compounds strongly contributed to the thermoelectric performance characterized by high thermal power in the p region. The optical and thermoelectric study carried out by J. Wei and G. Wang **[20]** on the TaCoSn HH alloy showed a powerful light adsorption capacity in the visible zone, which is of 125.10^4 cm^{-1}. The results of transport properties show that TaCoSn exhibits an excellent thermoelectric performance characterized by a high Seebeck coefficient and merit factor. In an experimental study carried out by W. Silpawilawan et al., **[21]**, the nanostructured $Nb_{0.9}Ti_{0.1}FeSb$ was synthesized by melt spinning followed by spark plasma sintering. An improvement of 20% in the ZT value was achieved, amelioration due to the reduction in thermal conductivity caused by this nanostructuring, which allow to effective phonon scattering. They declare that the NbFeSb remain one of the best p-type HH alloys in thermoelectric. Currently, the development of embedded systems engineering go through the search of the innovative (semiconductors, half-metallic) materials able to carry out actions in real time. For this it is necessary that these compounds will have high optical, thermoelectric and spintronic performances. It is in this perspective that we are going in this research to emphasize the thermoelectric and optical responses of four new semiconductors possessing 18 valence electrons.

Cite as: B.S. Ahmed, B. Anissa, D. Radouan, N. Al Bouzieh, I.K. Durukan, N. Amrane, East Eur. J. Phys. 1, 294 (2024), https://doi.org/10.26565/2312-4334-2024-1-26
© B.S. Ahmed, B. Anissa, D. Radouan, N. Al Bouzieh, I.K. Durukan, N. Amrane, 2024; CC BY 4.0 license

2. COMPUTATIONAL METHOD

In this work, all properties of the H.H compounds XRhZ (X = V, Nb and Z = Si, Ge) have been studied with WIEN2k code **[22]** which is based on DFT calculations **[23]**. The computations were determined by full potential linearized augmented plane wave method **[24]**. Among the exchange-correlation functionals, the generalized gradient approximation (GGA) **[25-26]** and the Tran and Blaha modified Becke-Johnson method (TB-mBJ) **[27]** were retained for this study. The H.H have the C_{1b} crystal structure with the space group F-43m. The muffin tin radius (RMT) values of 2.5, 2.1 and 1.9 a.u were used for for X, Rh and Z elements. Other input data, such as k-point mesh (K_{MAX}), RMT*wave-vector, Gaussian parameter and the maximum angular momentum were selected to 14*14*14 **[28]**, 7.0, 12 and 10 respectively. The value of -6.0 Ry is taken as the energy of the interval between the core and valence states and the energy convergence criterion of 10^{-4} Ry is adopted for the self-consistent field calculations. The electron transport properties are determined under a fine mesh of 46×46×46 **[29]** by the semi-classical Boltzmann transport equation (BTE) as given in the BoltzTraP code **[30]**. The optical responses of our new compounds were determined by the complex dielectric function **ε(ω)** as given from the Kramer–Kronig relation **[31-33]**.

3. RESULTS AND DISCUSSIONS

3.1 Structural properties and phase stability

The H.H compounds XRhZ (X = V, N*b* and Z = Si, Ge) crystallizes in the face centered cubic space group (F43m). The Silicon (Germanium) and Vanadium (Niobium) atoms are located at the octahedral 4b (1/2, 1/2, 1/2) and 4a (0, 0, 0) Wyckoff positions, while the Rhodium element occupies tetrahedral position 4c (1/4, 1/4, 1/4). The unit cell structure of the XRhZ compound plotted using Vesta 4.5 software **[34]** is shown in **Figure 1**. We can observe that the arrangement contains three interpenetrating ordered fcc sublattices which are occupied by X, Rh and Z atoms respectively. The covalent nature of the [XZ] sublattice is emphasized as a zinc blende sublattice, while the Rh and Z atoms form a rock salt structure.

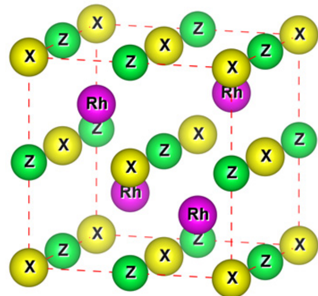

Figure 1. Crystalline structure of *XRhZ (X =V, Nb and Z = Si, Ge)*

The NaCl-type substructure consisting of atoms with large electronegativity difference implies strong ionic bonding character, while the ZnS-type substructure, which involves strong covalent character, consists of atoms having a smaller difference in electronegativity **[35]**. **Table 1** gives the structural parameters of VRhSi, VRhGe, NbRhSi and NbRhGe H.H. compounds calculated by using the GGA approximation in the ferromagnetic and nonmagnetic states. The main parameters are the bulk modulus **B**, its pressure derivative **B'**, the equilibrium lattice constant $\boldsymbol{a_0}$, cohesive energy $\boldsymbol{E_{coh}}$, formation energy $\Delta\boldsymbol{H_f}$ and ground state energy $\boldsymbol{E_{min}}$. For the four alloys, the **γ**-phase is energetically more stable than **α** and **β** phases, in addition this most stable state, was found to be nonmagnetic. The calculated lattice parameters values are 5.71 Å, 5.80 Å, 5.91Å and 5.97 Å respectively for VRhSi, VRhGe, NbRhSi and NbRhGe compounds. These values are in perfect harmony with those of other semiconducting H.H alloys with VEC of 18, let's quote TaCoSn (5.94 Å) **[36]**, NbIrGe (6.02 Å) **[18]**, HfCoSb (6.04 Å) **[37]**.

The experimental synthesis of the H.H compounds XRhZ (X = V, Nb and Z = Si, Ge) compounds is only possible if the formation energy value $\Delta\boldsymbol{H_f}$ calculated according to relation (1) is negative **[38]**.

$$\Delta \boldsymbol{H_f} = \boldsymbol{E_{XYZ}^{tot}} - \left(\boldsymbol{E_X^{bulk}} + \boldsymbol{E_Y^{bulk}} + \boldsymbol{E_Z^{bulk}}\right). \tag{1}$$

Where $\mathbf{E^{bulk}}$ is the energy per atom of constituent atoms in bulk and $\boldsymbol{E_{XYZ}^{tot}}$ is the total energy of primitive cell. Negative values of the formation energy obtained for all the four H.H, confirms that the synthesis of these compounds remain possible. To predict the stability of the H.H alloys XRhZ (X = V, Nb and Z = Si, Ge), we have calculated according to the relation (2) the corresponding cohesion energies **[39]**.

$$\boldsymbol{E_{coh}} = \boldsymbol{E_{XYZ}^{tot}} - \left(\boldsymbol{E_X^{iso}} + \boldsymbol{E_Y^{iso}} + \boldsymbol{E_Z^{iso}}\right). \tag{2}$$

Where $\mathbf{E^{iso}}$ is the isolated atom energy. The negative cohesive energies achieved justify that our four H.H are structurally stable. The calculation of phonon dispersion in the first Brillouin zone along the high-symmetry points is given for the studied compounds thanks to the Phono3py code **[40]**. The phonon band structures of NbRhGe compound is already given in previous study conducted by Y.Wang **[18].** The absence of imaginary phonon frequency in whole Brillioun zone **(Fig. 2)** confirms the dynamical stability of our semiconductor's compounds in their ground states.

Table 1. Calculated structural equilibrium lattice constant a **(A°)**, pressure derivatives B', ground state energies E_{min} **(Ry)**, formation energy ΔH_f **(Ry)** and cohesive energy E_{coh} **(Ry)**

Alloys	State	Type	a	B'	Emin	E_{coh}	ΔH_f
VRhSi	FM	α	5.72	3.91	-12049.276632		
	NM		5.72	3.09	-12049.276687		
	FM	β	5.69	4.09	-12049.302767		
	NM		5.70	3.01	-12049.303182		
	FM	γ	5.73	3.86	-12049.366754		
	NM		**5.71**	**4.49**	**-12049.367117**	**-1.4227**	**-0.199**
VRhGe	FM	α	5.81	5.87	-15667.350805		
	NM		5.81	5.20	-15667.350475		
	FM	β	5.79	6.56	-15667.341261		
	NM		5.81	6.41	-15667.341583		
	FM	γ	5.80	6.77	-15667.410282		
	NM		**5.80**	**6.03**	**-15667.422243**	**-1.2878**	**-0.844**
NbRhSi	FM	α	6.01	4.40	-17791.550849		
	NM		6.01	4.27	-17791.551936		
	FM	β	5.87	4.31	-17791.605674		
	NM		5.88	4.30	-17791.606164		
	FM	γ	5.92	4.72	-17791.690152		
	NM		**5.91**	**5.21**	**-17791.692559**	**-1.4905**	**-0.237**
NbRhGe	FM	α	6.09	6.01	-21409.636669		
	NM		6.09	5.98	-21409.636659		
	FM	β	5.97	5.30	-21409.652489		
	NM		5.97	5.34	-21409.652959		
	FM	γ	5.98	5.75	-21409.754550		
	NM		**5.97**	**4.26**	**-21409.754950**	**-1.3619**	**-0.868**

Phase α : X (1/4, 1/4, 1/4) Y (1/2, 1/2, 1/2) Z (0, 0, 0)
Phase β : X (1/2, 1/2, 1/2) Y (0, 0, 0) Z (1/4, 1/4, 1/4)
Phase γ : X (0, 0, 0) Y (1/4, 1/4, 1/4) Z (1/2, 1/2, 1/2)

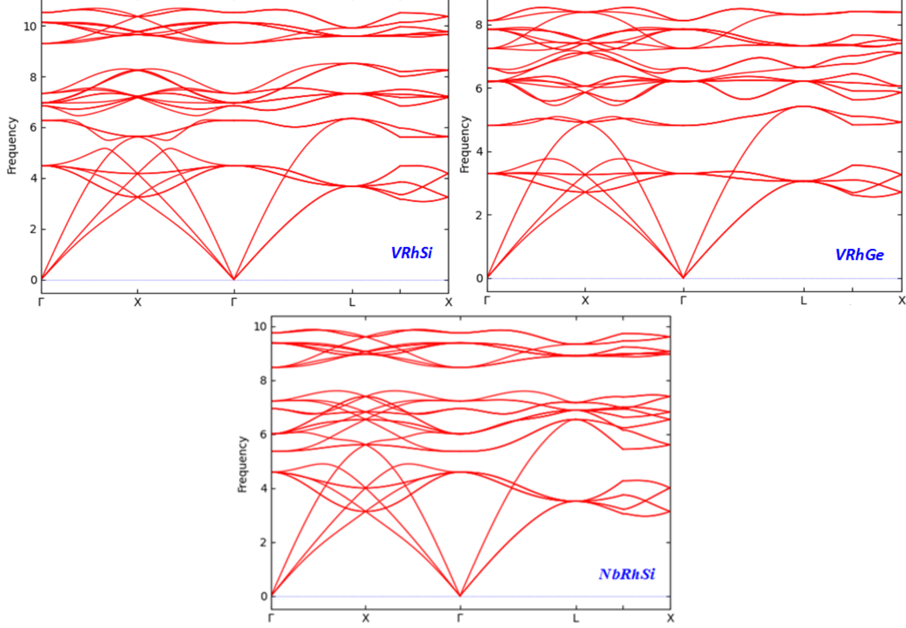

Figure 2. The phonon band structures of (a) *VRhSi,* (b) *VRhGe and* (c) *NbRhSi*

The acoustic modes exhibit the high dispersions, which means that they contribute well to the heat transport while the optical modes contribute little to the heat transport due to their weak dispersion. For the VRhSi and VRhGe, we see an overlap of acoustic and optical branches near X and L points thus indicating the strong phonon–phonon scattering **[41]**.

3.2 Electronic properties

The magnetic performance of ternary H.H is estimated by the Slater-Pauling equation **[42]**.

$$M_t = (18 - Z_t) \tag{3}$$

Z_t and M_t denote respectively the total number of valence electrons in the unit cell and the total magnetic moment. The explicit valence electrons for the XRhZ (X=V, Nb and Z=Si, Ge) primal cell are V: [Ar] $3d^3$ $4s^2$, Nb: [Kr] $3d^4$ $5s^1$, Rh: [Kr] $4d^8$ $5s^1$, Si: [Ne] $3s^2 3p^2$ and Ge: [Ar] $3d^{10}$ $4s^2$ $4p^2$. At first sight and according to the relation (3), the four compounds studied in this research do not exhibit magnetism, because they all have 18 electrons in their valence shell. The calculation of their total magnetic moment shows that these compounds are not magnetic ($M_t = 0\ \mu B$), thus confirming the result already predicted by the optimization. The electronic band structures (EBS) of VRhSi, NbRhSi, VRhGe and NbRhGe H.H alloys was carried out at the equilibrium lattice parameters by TB-mBJ approach.

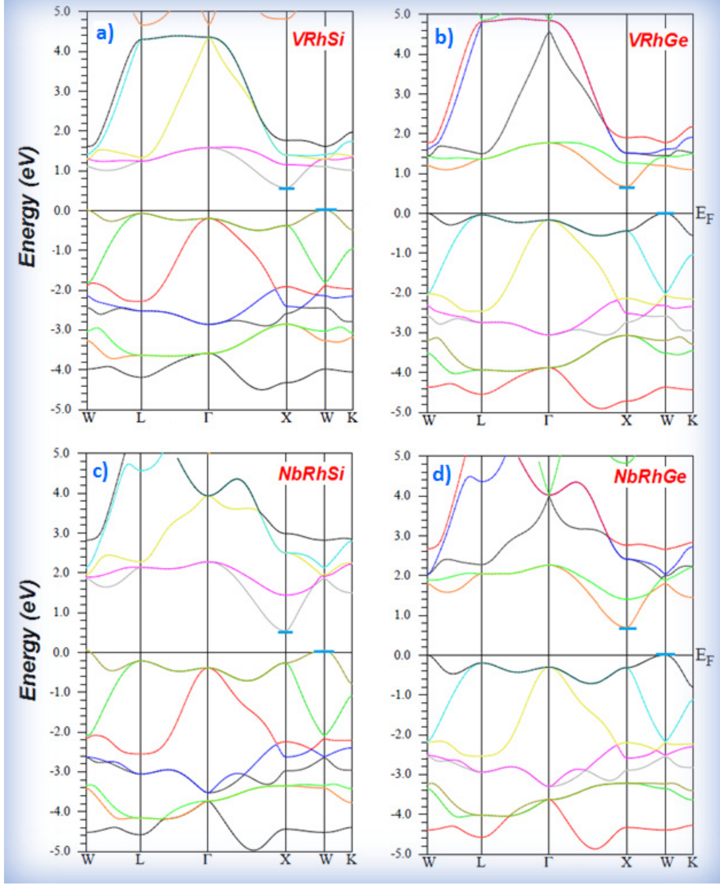

Figure 3. Band structures of (a) VRhSi, (b) NbRhSi, (c) VRhGe, (d) NbRhGe

The EBS diagrams **(Fig. 3a-d)** reveal for the studied compounds, that the top of valence band is located at W symmetry point while the bottom of conduction band is located at X-symmetry point. All the materials exhibit semiconductor nature with narrow indirect band gap of 0.59, 0.68, 0.51 and 0.71 eV for VRhSi, NbRhSi, VRhGe and NbRhGe respectively. These findings are in good adequacy with other fundamental results obtained for H.H semiconductors having the same X atom that our alloys, let us quote the NbIrGe (0.63 eV) **[18]**, VRuSb (0.64 eV) **[16]**, NaScSi (0.61 eV) **[43]**. We can observe from the BS plots that the L and Γ are the points for the valence bands convergence and that the distribution of these bands is mainly due to the heavy hybridization of the d states of the X (V, Nb) and Z (Si, Ge) atoms. The energy difference between the W and L points for the NbRhSi and NbRhGe compounds is around 0,16 and 0.18 eV while for the VRhSi and VRhGe compounds this difference is negligible. The four compounds show a triple band degeneracy at Γ point while L point show a double band degeneracy. This degeneracy of the valence band at the $\mathbf{E_F}$ constitutes an index of a good thermoelectric performance of the studied materials. To better comprehend the band diagrams of XRhZ (X=V, Nb and Z=Si, Ge) compounds, we have computed using the TB-mBJ method their total (TDOS) and partial densities of states (PDOS). Based on the TDOS/PDOS spectra (**Fig. 4a-d**), we can notice that the four H.H alloys, show almost similar profile in valence and conduction band. For the VRhSi/VRhGe compound, the valence band maximum (VBM) is composed of V-3d states, Rh-4d states and a small dispersion of Si-3p (Ge-3p) states, while the conduction band minimum (CBM) is mainly constituted of V-3d states.

For the NbRhSi and NbRhGe compounds, the strong contribution below $\mathbf{E_F}$ comes from the Nb-4d state while the states above $\mathbf{E_F}$ are mainly due to the Nb-4d and Rh-4d states and to a small contribution of the Si-3p (Ge-3p) states. The p-type doping could have the capacity to contain more charge carriers than n-type doping **[44]** since around the Fermi level, the TDOS of the valence band is larger than that of the conduction band. From the PDOS plots, one can conclude for the four materials, that the X-d states and Rh-d states give the main contribution to conductivity, while the Ge-p and Ge-s states have no influence on transport properties.

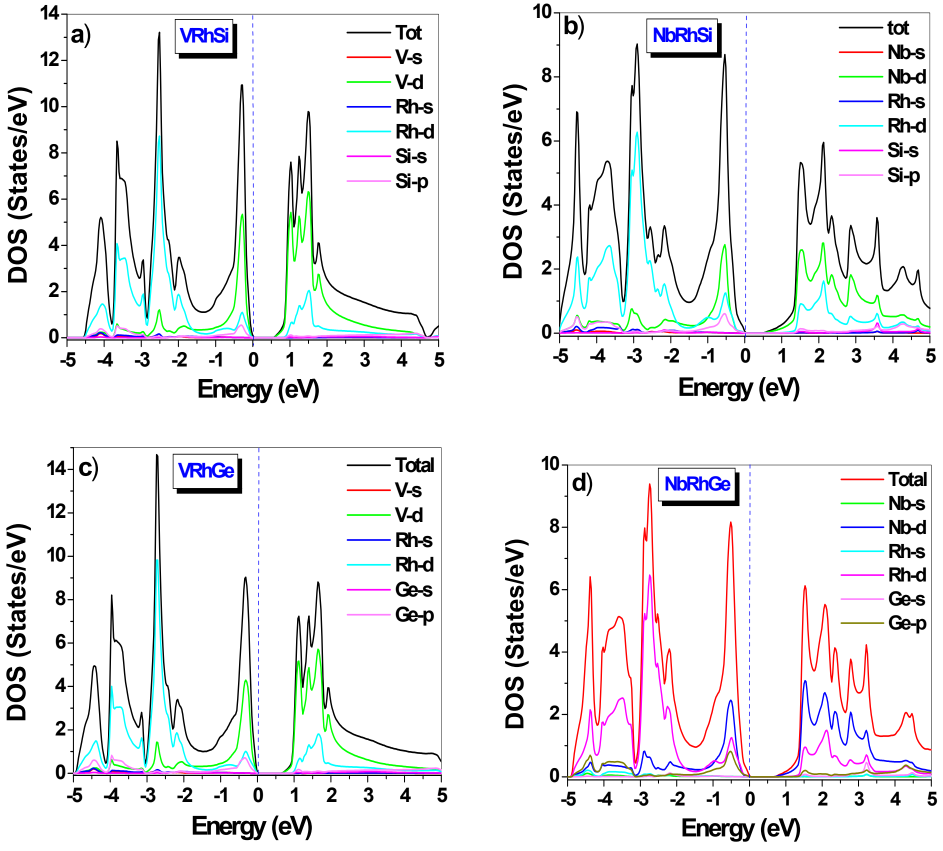

Figure 4. Total and partial density of states (TDOS / PDOS) of (a) VRhSi, (b) NbRhSi, (c) VRhGe, (d) NbRhGe.

3.3 Elastic properties

Examining the mechanical stability of H.H alloys XRhZ (X = V, Nb and Z = Si, Ge) requires the knowledge of the three elastic constants C_{11}, C_{12}, C_{44} **[45]**. These constants allow to estimated according to the equations (4) to (8), the bulk modulus B, the shear modulus G, Young's modulus E, Poisson's ratio ν and the elastic anisotropy factor A **[46]**.

$$B = \frac{1}{3}(C_{11} + 2C_{12}), \quad (4)$$

$$G = \frac{C_{11} - C_{12} + 3C_{44}}{5}, \quad (5)$$

$$E = \frac{9BG}{3B + G}, \quad (6)$$

$$\nu = \frac{3B - E}{6B}, \quad (7)$$

$$A = \frac{2C_{44}}{C_{11} - C_{12}}. \quad (8)$$

From **Table 2,** which gives the independent elastic constants, we can conclude that at zero pressure, the H.H compounds XRhZ (X = V, Rh and Z = Si, Ge) are mechanically stable due to the fact that they satisfy all of Born's elastic stability criteria **[47]** $\mathbf{(C_{11} - C_{12} > 0)}$; $\mathbf{(C_{11} + 2C_{12} > 0)}$; $\mathbf{(C_{11} > 0)}$; $\mathbf{(C_{44} > 0)}$ and $\mathbf{(C_{12} < B < C_{11})}$. For the alloys treated in this research, the condition $\mathbf{C_{11} > C_{22} > C_{33}}$ was established, this confirms that XRhZ (X = V, Rh and Z = Si, Ge) alloys are most tough to the unidirectional compression than shear deformation. Compared to the three other H.H, the VRhGe show a low value of bulk modulus (B) which mean that this material is easy to compress. The shear modulus (G) describes the resistance of the material against permanent deformation due to a shear stress. Based on our calculations, NbRhSi has higher Shear modulus (65.22 GPa), so a higher hardness among other alloys, while the VRhSi has the lowest hardness (52.21 GPa). The ability of a material to resist changes in its length when subjected to longitudinal compression is defined by Young's modulus (E). Based on our calculations, NbRhSi has the highest Young modulus (167.26 GPa) so a highest stiffness and VRhSi has the lowest stiffness among the four studied alloys. According to the obtained values of G and E, the NbRhSi compound can be classified as a high rigidity hard material. The range of values found for shear moduli and Young's moduli is in agreement with those of several HH compounds cited in the literature **[48-50]**.

Table 2. The computed elastic constants *Cij* $(\boldsymbol{GPa})$, bulk modulus $B(\boldsymbol{GPa})$, Shear modulus $G(\boldsymbol{GPa})$, Young's modulus E $(\boldsymbol{GPa})$, Poisson's ratio (ν), anisotropic factor A, and Pugh's ratio (*B/ G*) of VRhZ (Z =C, Si, Ge) half-Heusler materials

	C_{11}	C_{12}	C_{44}	B	G	E	ν	A	B/G
VRhSi	147.47	102.06	66.84	112.15	52.21	135	0.30	2.21	2.14
VRhGe	133.30	80.19	75.12	97.90	55.69	140	0.26	2.83	1.76
NbRhSi	176.39	109.98	82.34	127.92	65.22	167	0.28	2.08	1.96
NbRhGe	173.21	104.61	78.27	127.47	60.68	157	0.29	2.28	2.10

Poisson's ratio (ν) values obtained are located between 0.26 and 0.30, which confirms according to Haines et al. **[51]** the presence of covalent and metallic bonding (ν < 0.33). The VRhSi, VRhGe, NbRhSi and NbRhGe compounds present an anisotropy coefficient (A) different from unity (**Table 2)**, which confirms their anisotropic mechanical behavior. The risk of micro cracking within these compounds is minimal given that their degree of anisotropy is low. Other important characteristics, the ductility and fragility which are an intrinsic property of materials and which requires their determination in order to position material for a given application. According to Pugh's criterion **[52]**, the material behaves in brittle manner when B/G is lower than 1.75 and as ductile manner for B/G higher than 1.75. For the present investigation based on first principles calculations, we noted that the four studied compounds show B/G values greater than 1.75, suggesting the ductility of these HH.

3.4 Thermoelectric properties

The thermoelectric properties such as the Seebeck coefficient (S), thermal conductivity (κ/τ), electrical conductivity (σ/τ), and Merit factor (ZT) are calculated using the BoltzTraP code. All these properties are studied as a function of chemical potential change (μ). The change of (μ) can influences the stability of the materials during doping even if the electronic band remains unchanged **[53-54]**. In addition, these properties will be given versus temperature for chemical potential equal to Fermi energy. The most remarkable thermoelectric properties given by equations (9 to 12) all derive from the semi-classical Boltzmann transport equation **[55-56]**.

$$\boldsymbol{\sigma_{\alpha\beta}(T,\mu) = \frac{1}{\Omega}\int \sigma_{\alpha\beta}(\varepsilon)\left[-\partial f_{\mu}(T,\varepsilon)\right]d\varepsilon}, \quad (9)$$

$$\boldsymbol{\kappa_{\alpha\beta}(T,\mu) = \frac{1}{e^2 T\Omega}\int \sigma_{\alpha\beta}\varepsilon(\varepsilon-\mu)^2 \ \frac{\partial f_{\mu}(T,\varepsilon)}{d\varepsilon}}, \quad (10)$$

$$\boldsymbol{S = \frac{e}{T\sigma}\int \sigma_{\alpha\beta}(\varepsilon)(\varepsilon-\mu)\left[\frac{-\partial f_{\mu}(T,\varepsilon)}{\partial\varepsilon}\right]}, \quad (11)$$

$$\boldsymbol{ZT = \frac{S^2\sigma T}{\kappa}}. \quad (12)$$

Where $\boldsymbol{\sigma, \mu, \Omega, f, \kappa, S}$ and $\boldsymbol{ZT}$ denotes respectively electrical conductivity, chemical potential, unit-cell volume, Fermi-Dirac distribution function, thermal conductivity, Seebeck coefficient and merit factor.

The knowledge of the temperature effect on thermoelectric properties is a crucial key for identifying the reliability of compounds in thermoelectric applications. The variation of Seebeck coefficient which provides us the insight of the type of charge carriers in XRhZ (X=V,Nb and Z=Si,Ge) compounds, have been drawn versus temperature (**Fig. 5a)**. In all considered temperature range, the sign of S is positive, thus meaning that the holes are the majority charge carriers. For VRhGe H.H, the S value increases to its utmost value of 270 $\mu V \cdot K^{-1}$ at 300 K then decrease to achieve 221 $\mu V \cdot K^{-1}$ at 1200 K, while for the NbRhGe compound, S increases up to a maximum value of 261 $\mu V \cdot K^{-1}$ at 900 K and then decreases weakly to reach 254 $\mu V \cdot K^{-1}$ at 1200 K.

For the VRhSi alloy, the value of S goes from 240 $\mu V \cdot K^{-1}$ at 300K to 269 $\mu V \cdot K^{-1}$ at 700K then drops again to 240 $\mu V . K^{-1}$at 1200K. The utmost value of "S" for the NbRhSi alloy is observed at 900 K it is of 262 $\mu V . K^{-1}$. Around room temperature, "S" shows a large positive value of about 270 μV/K, 240 μV/K and 225 μV/K respectively for VRhGe, NbRhSi/VRhSi and NbRhGe. The trend of Seebeck coefficient with respect to chemical potential **(μ)**, has been displayed in **Fig. 6a** and **Fig. 7a**. At room temperature, the peaks of S are obtained at μ values included between -0.03 to 0.01 eV for VRhGe/NbRhGe and between -0.02 to 0.01 eV for VRhSi/NbRhSi compound. Beyond these range of μ, S tends to zero. With rising in the temperature, the maximum value decreases, it goes from 1205μV/K at 300K to 473μV/K at 900K for VRhGe/NbRhGe and from 853μV/K at 300K to 384μV/K at 900K respectively for VRhSi/NbRhSi compounds. The optimal values of S occur on the negative side of **μ**. Above the room temperature, S gradually decreases with the rise in temperature; this is due to jumping of electron and hopping of holes around the localized states in the vicinity of $\mathbf{E_F}$ **[57]** which will generates a rise in the thermal energy. Comparatively to VRhSi and NbRhSi compounds, the VRhGe and NbRhGe H.H are well suitable for thermoelectric devices working around 300 K, since their maximum Seebeck values are reached at 300 K.

From **Fig. 5b** which give the evolution of electrical conductivity (σ/τ) versus temperature, we can see that σ/τ increases as temperature increases, suggesting the semiconducting nature of XRhZ (X=V,Nb and Z=Si,Ge) compounds. For all the studied compounds, the σ/τ value is almost similar up to room temperature, above 300 K a strong increase is

observed for the VRhGe compound. The lowest values of σ/τ are obtained at 100 K, they are around 6×10^{17} $(\Omega ms)^{-1}$, while the maximum values are obtained at 1200 K they're from 4.61×10^{19} $(\Omega ms)^{-1}$ for VRhGe and around 3×10^{19} $(\Omega ms)^{-1}$ for VRhSi, NbRhGe and NbRhSi. The effect of chemical potential (μ) on the electrical conductivity (σ/τ) of the H.H compounds XRhZ (X = V, Nb and Z = Si, Ge) is drawn in **Fig. 6b** and **Fig. 7b**.

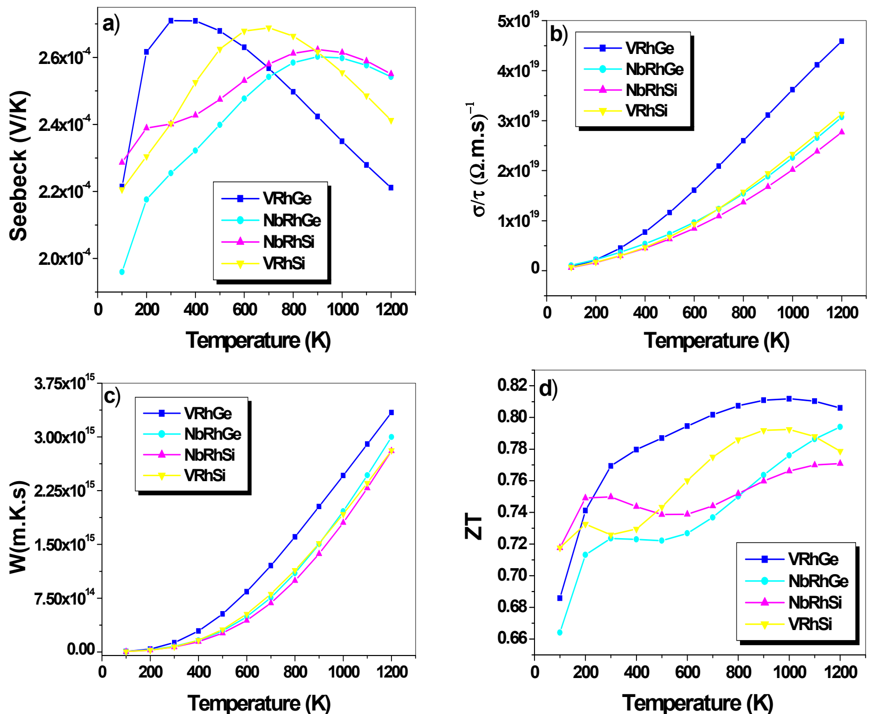

Figure 5. Evolution versus temperature of (a) Seebeck coefficient, (b) electrical conductivity, (c) thermal conductivity and (d) Merit factor of *XRhZ (X =V, Nb and Z = Si, Ge)*.

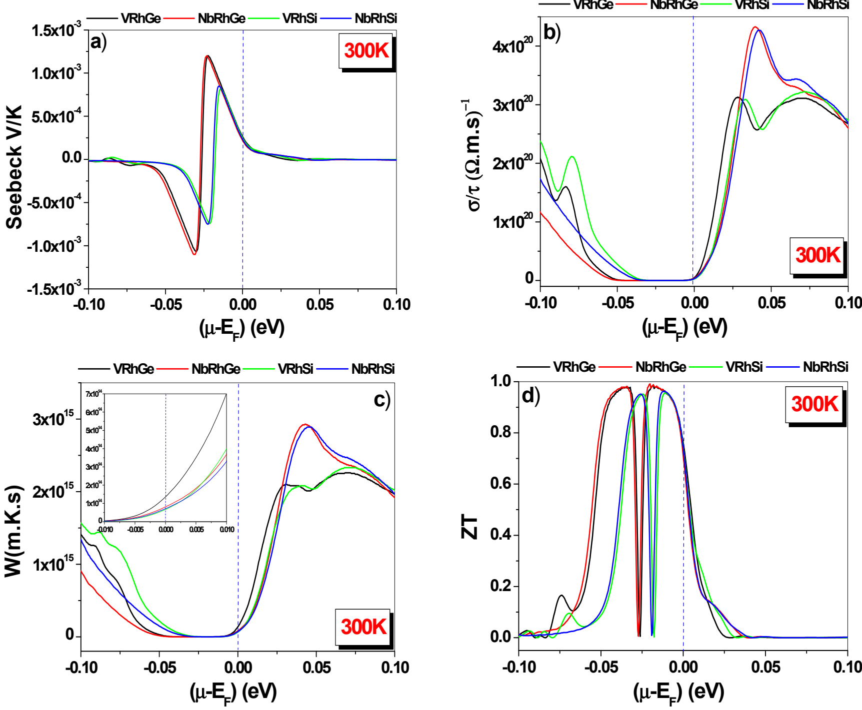

Figure 6. Evolution versus chemical potential of (a) Seebeck coefficient, (b) electrical conductivity, (c) thermal conductivity and (d) Merit factor of *XRhZ (X =V, Nb and Z = Si, Ge)*. (T= 300K)

Comparatively to the p-type region, the electrons in n-type region show at room temperature dominancy with maximum peak intensity of 3.12×10^{20} $(\Omega\ m\ s)^{-1}$ / 4.32×10^{20} $(\Omega\ m\ s)^{-1}$ occurring at -0.028 eV / (-0.039 eV) respectively for NbRhSi/NbRhGe and VRhSi/VRhGe compounds. Almost the same result is obtained at 900K. For the temperatures

of 300 and 900 K, we notice that the profiles of σ/τ do not show any major change, the curves are almost confused except for a few small differences. The high values of σ/τ recorded for the four H.H denote the low losses by Joule effect; this is explained by the difference between the effective masses of electrons (conduction band) which are heavier than the effective masses of holes (valence band). From **Fig. 5c**, which depict the comportment of electronic thermal conductivity $(\boldsymbol{\kappa_e/\tau})$ as function of temperature, one can notice that $\boldsymbol{\kappa_e/\tau}$ increases almost linearly with temperature. At ambient temperature the $\boldsymbol{\kappa_e/\tau}$ is of 1.29×10^{14} for VRhGe and around 7.80×10^{13} for the other three compounds. For the materials studied in this paper, the lowest values of **κ/τ** are obtained at 100 K, while the maximum values are obtained at 1200 K. At the same chemical potential, the gap between the values of $\boldsymbol{\kappa_e/\tau}$ increase as temperature increase, but with a gradient of less importance than that of the electrical conductivity **σ/τ** case. According to the **Fig. 6c** and **Fig. 7c**, which illustrates the thermal conductivity $\boldsymbol{\kappa_e/\tau}$ given versus chemical potential μ(eV), we can reveal the clear amplification of $\boldsymbol{\kappa_e/\tau}$ when the temperature increases. The $\boldsymbol{\kappa_e/\tau}$ is higher for the p-type (electrons) than for the n-type (holes). At ambient temperature and for **μ=E$_F$**, the $\boldsymbol{\kappa_e/\tau}$ value is of $1,34\times10^{14}$ W/m.K.s for VRhGe and around $7,50\times10^{13}$ W/m.K.s for the other three compounds. The values of **κ/τ** are larger for $\mu > 0$ than for $\mu < 0$. At room temperature, the VRhSi and theVRhGe compounds exhibit a low thermal conductivity peak, which mean that these two H.H can provide high thermal efficiency. The high merit factor (ZT) values obtained constitute a strong index of the high thermoelectric performance of these materials. In fact, this parameter highly depends on the temperature, thermal conductivity (κ/τ), electrical conductivity (σ/τ) and Seebeck coefficient (S). **Fig. 5d** gives the evolution of merit factor (ZT) versus temeprature at μ=E$_F$. Electrons nearby the **E$_F$** play an essential role in the transport properties. ZT value of the VRhGe alloy remain the best among the four studied compounds, it increase from 0.68 at 100 K to its utmost value of 0.81 at 1000 K while at room temperature its value is of 0.77. Beyond 200 K, all the compounds have a ZT value that is greater than 0.71. From **Fig. 6d** and **Fig. 7d**, which give the change of ZT regarding the chemical potential, one can see that the values of ZT are lower in the p-type region than in the n-type region and as the temperature tends toward 300K, the utmost value of ZT progressively increases. At room temperature, the ZT values is around the unity, which makes the XRhZ (X=V,Nb and Z=Si,Ge) compounds very attractive for thermoelectric devices working at room temperature. We have identified in the literature several H.H semiconductors, which are classified as a good thermoelectric material and which exhibit the almost same values of ZT than our studied alloys, let's quote TiIrAs, TiIrSb **[58]**.

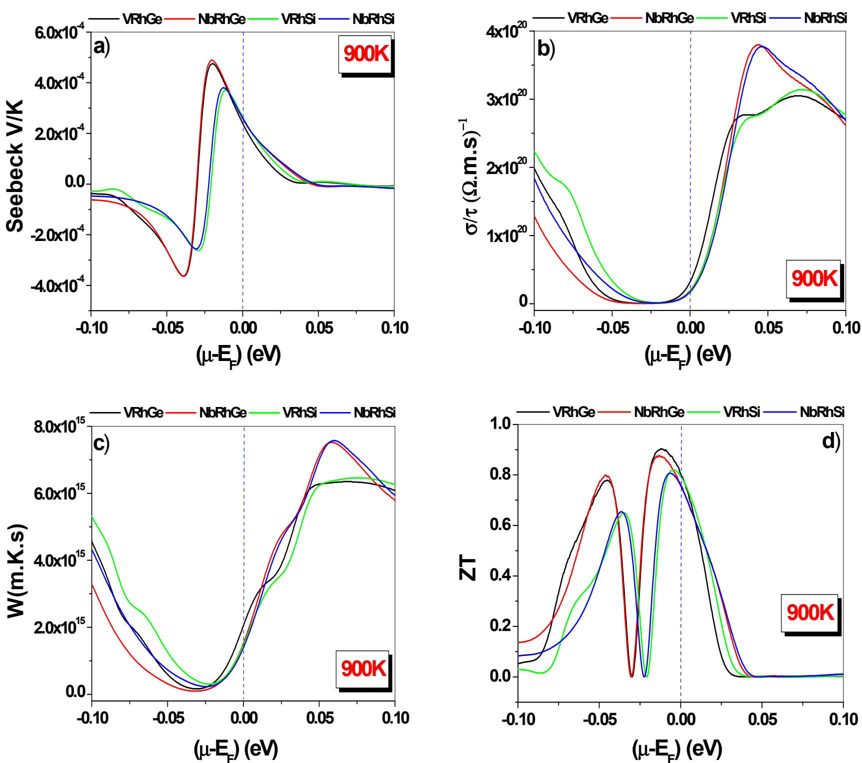

Figure 7. Evolution versus chemical potential of (a) Seebeck coefficient, (b) electrical conductivity, (c) thermal conductivity and (d) Merit factor of *XRhZ (X =V, Nb and Z = Si, Ge)*. (T= 900K)

3.5 Optical properties

Even though the semiconductor compound is known to be a very good material for optical applications, its optical study is considered necessary, because this type of material can lose its semiconductor characteristic at very low frequency and become metallic as it can also acquire the behavior of an insulator at very high frequency **[59]**. The majority of the optical characteristics come from the dielectric complex function $\boldsymbol{\varepsilon(\omega)}$ **(eq.13) [33]**.

$$\varepsilon(\omega) = \varepsilon_1(\omega) + i\varepsilon_2(\omega) \tag{13}$$

$\varepsilon_1(\omega)$ describes the dispersion of electromagnetic radiation whereas $\varepsilon_2(\omega)$ represents the optical absorption of the material.

The imaginary part of the dielectric function $\varepsilon_2(\omega)$ comes from the EBS computations with the help of the following relation

$$\varepsilon_2(\omega) = \left(\frac{4\pi^2 e^2}{m^2\omega^2}\right)\sum_{i,j}\int \langle i|M|j\rangle^2 f_i(1-f_i)\delta(E_j - E_i - \omega)d^3k. \tag{14}$$

Where ω, e, m and M denote respectively the photon frequency, electron charge, electron mass and dipole matrix. E_j designates the final state electron energy, E_i the initial state electron energy and f_i the Fermi occupation factor of the single-particle state i.

Thanks to the Kramer's Kronig relations **[60-61]**, the real part of the dielectric function $\varepsilon_1(\omega)$ is deduce from the imaginary part of the same function $\varepsilon_2(\omega)$.

$$\varepsilon_1(\omega) = 1 + \frac{2}{\pi}P\int_0^\infty \frac{\omega'\varepsilon_2(\omega')}{\omega'^2 - \omega^2}d\omega'. \tag{15}$$

Where P represents the principal Cauchy value. Additional optical quantities can be also deduced from the calculated values of the imaginary and real parts of the dielectric function **[62]**, the most sought after among them are the reflectivity $R(\omega)$, the refractive index $n(\omega)$ and the absorption coefficient $a(\omega)$**.** The crystallographic structures of the studied compounds are cubic; hence, the optical properties will be isotropic. In order to reach sensible accuracy on all probable electronic transitions, a dense mesh is considered necessary. A k-point mesh of 31*31*31 was adopted in this part of optical calculation. The various optical properties examined using the TB-mBJ method are plotted in the near infrared (NIR), visible (Vis) and ultraviolet (UV) domains.

$$R(\omega) = \left|\frac{\sqrt{\varepsilon(\omega)} - 1}{\sqrt{\varepsilon(\omega)} + 1}\right|^2 \tag{16}$$

$$n(\omega) = \left[\frac{\sqrt{\varepsilon_1{}^2(\omega) + \varepsilon_2{}^2(\omega)} + \varepsilon_1(\omega)}{2}\right]^{1/2} \tag{17}$$

$$a(\omega) = \frac{\sqrt{2\omega}}{c}\left(\sqrt{\varepsilon_1^2(\omega) + \varepsilon_2^2(\omega)} - \varepsilon_1(\omega)\right)^{1/2} \tag{18}$$

The graphical plot of **Fig. 8a** gives the real part of dielectric function $\varepsilon_1(\omega)$; part, which defines the extent a material, may be polarized. Comparatively to the visible and infrared regions, the H.H compounds XRhZ (X = V, Nb and Z = Si, Ge) react highly to the ultraviolet-light excitations; many peaks are detectable in this domain. The negative values of $\varepsilon_1(\omega)$ mean that the material entirely reflects the incident radiation while the positive values mean that the photons move across the material. For the VRhGe compound, the negative values of $\varepsilon_1(\omega)$, recorded between 1.97 and 2.40 eV (visible region) can be explained by the metallic character characterized by the reflection of incident radiation. The same observation was found for the VRhSi, NbRhGe and NbRhSi compounds in the energy ranges between 1.83 to 2.23 eV / (2.62 to 3.05 eV) / (2.65 to 3.21 eV) respectively. Beyond 12.90 eV, the four compounds show values of real part $\varepsilon_1(\omega)$ fluctuating around zero. The static dielectric constant $\varepsilon_1(0)$ (dielectric function for zero photon energy) which is inversely proportional to the band gap **[63]** was found respectively equal to 190.11, 178.77, 23.62 and 22.88 eV for the VRhSi, VRhGe, NbRhSi and NbRhGe compounds. The transition between the occupied and unoccupied states is mostly insured by the imaginary part of dielectric constant $\varepsilon_2(\omega)$ **[64]**. From **Fig. 8b**, we can see that $\varepsilon_2(\omega)$ curve of VRhSi/VRhGe has three main peaks located at 0.24eV, 1.90eV and 3.98eV, while $\varepsilon_2(\omega)$ curve of NbRhSi/NbRhGe exhibits two main peaks positioned around 2.43eV and 4.92eV. According to the band structure plot of VRhSi/VRhGe (**Fig.3a-b**), the three highest peaks of $\varepsilon_2(\omega)$ correspond to the indirect interband transitions between W-X, L-X and Γ-X states. The two highest peaks for the NbRhSi/NbRhGe, compound correspond to the indirect interband transitions between W-X and L-X states (**Fig.3c-d**). We can noticed that above 8.8 eV, the optical activity of the four compounds considerably decreases. **Fig. 8c**, illustrates versus photon energy the evolution of absorption coefficient $a(\omega)$. For the four compounds, we can observe from 0 to 50 eV that there are no regions, where the compounds are optically transparent to radiation ($a(\omega) = 0$). The values of $a(\omega)$start from 0 eV and reaches in the ultraviolet region their maximums of 371.48 at 40.14eV (VRhSi/VRhGe) and 314.42 at 33.26 eV (NbRhSi/NbRhGe). Due to these high absorption values, these compounds may be beneficial to absorb harmful UV rays. In the visible region, the maximum values of $a(\omega)$ is about 112.84 cm^{-1} for NbRhSi/NbRhGe, and about 84.26 cm^{-1} for VRhSi/VRhGe. These values are larger to those reported for many H.H semiconductors

compounds such as LiCaX (X=N, P and As) **[65]**, ZrRhSb **[66]**, XScZ (X = Li, Na; Z = C, Si, Ge) **[67]**, RbScSn **[68]** and SiLiX (X = Ca and Sr) **[69]**. The evolution of light reflection $\boldsymbol{R(\omega)}$ versus photonic energy is illustrated in **Fig. 8d**.

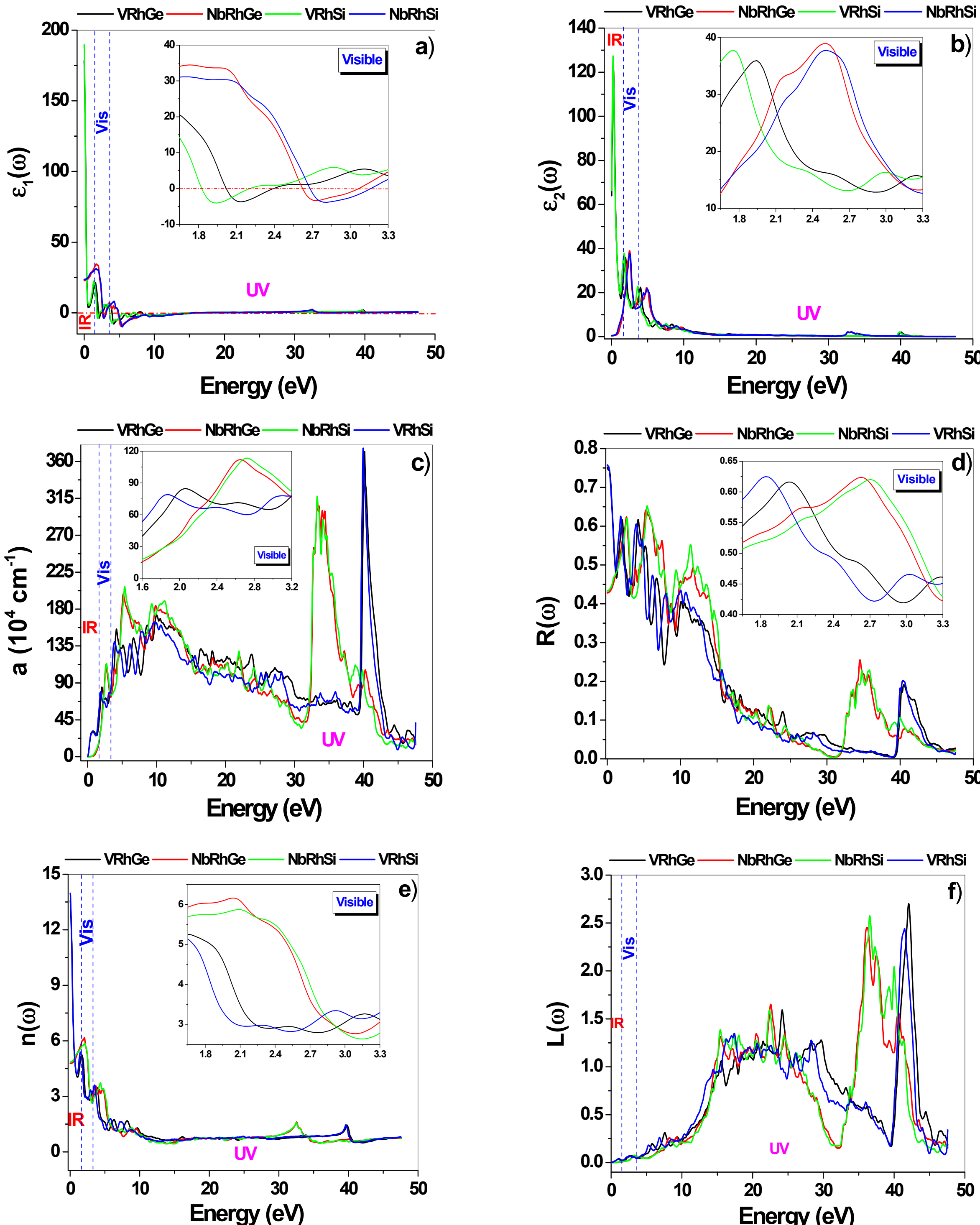

Figure 8. Illustration of (a) real $\varepsilon_1(\omega)$ and (b) imaginary $\varepsilon_2(\omega)$ component of dielectric function, (c) absorption coefficient a(ω), (d) reflectivity R(ω), (e) refractive index n(ω), and (f) electron energy loss L(ω) for *XRhZ (X =V, Nb and Z = Si, Ge)*

We can see that at zero energy, $\boldsymbol{R(0)}$ is relatively high for VRhSi /VRhGe its value is of 75% while that of NbRhGe/NbRhGe is of 43%. Over low energies, $\boldsymbol{R(\omega)}$ oscillates and the highest value for the VRhGe is obtained in the visible domain (62 %), while the utmost value for the NbRhGe which is of 64 % has registered in the UV domain. A value of $\boldsymbol{R}$ around 66% is observed in the UV domain for the alloys containing silicon (VRhSi and NbRhSi). The high-infrared reflectivity of approximately 75% makes VRhSi/VRhGe compounds ideal materials for use as high-performance heat shields. **Fig. 8e** shows the variation of refractive index versus phonon energy for the four

compounds studied in this research. We clearly notice that the $n(\omega)$shape is similar to that of $\varepsilon_1(\omega)$. For zero photon energy, the refractive index of VRhSi/VRhGe is significantly higher than, those of NbRhSi/NbRhGe. In addition, the real part of the dielectric constant $\varepsilon_1(0)$ and the refractive index $n(0)$ are obey to the equation $\varepsilon_1(0) = n^2(0)$ **[70]**. For the VRhSi/VRhGe compounds, the refractive index $n(\omega)$ starts rapidly to decrease before reached 1eV, then increases to attain its utmost value of 5.30 at 1.60 eV. While for the NbRhSi/NbRhGe compounds, a slight increase is noted between 0.14-1.96eV, beyond this range we observed a decrease of $n(\omega)$values to stabilize around 0.7. We notice that it is in the visible range that the utmost values of $n(\omega)$ occur. **Fig. 8f**, gives us the loss function energy $L(\omega)$; it can be seen that the prominent peaks of $L(\omega)$ for all four compounds are located in the high-frequency UV domain going from 15 eV to 42.0 eV. These peaks match to the fast decrease of the reflectivity $R(\omega)$. Also, the different peaks of $L(\omega)$ are directly related to the plasma resonance, in other words, to the state of electron vibrations in the valence band. In the infrared region and visible region, all the compounds exhibit a very weak energy loss.

CONCLUSIONS

In this manuscript, the structural, electronic, elastic, thermoelectric and optical behavior of ternary half-Heuslers XRhZ (X = V, Nb and Z = Si, Ge) in cubic phase have been studied and discussed using DFT methods. For all studied compounds, the structural optimization confirms that the NM state is more stable than the FM state, while the EBS and DOS graphs reveal non-magnetic semiconductor behavior. The negative values found for the formation enthalpy and cohesive energy are strong clues of the thermodynamic stability and possible structural synthesizability of these HH. The phonon band structures of XRhZ compounds show no imaginary frequency and testify to the dynamic stability of its semiconductors in the nonmagnetic γ phase. The elastic properties results showed that the four semiconductors are stable mechanically. They possess a low anisotropy degree therefore a minimal risk of micro cracking and they also revealed a ductile nature. The optical performances was studied in the energetic domain, ranging from 0 eV up to 50 eV. The high reflectivity greater than 60%, detected in the visible and UV areas as well as the high peaks of the absorption coefficient obtained in the same zones, allow using these alloys as UV filters, UV–visible photodetector, or as an effective shield in these domains. The increase in thermoelectric power generally passes through the decrease in thermal conductivity. For temperatures greater than 300K, the substitution of the germanium atom by the silicon atom (lighter atom) leads in a considerable reduction in thermal conductivity, reduction of 38% at 600K and 26% at 900K. With a merit factor values greater than 0.73 in wide temperature domain, all these compounds can be considered as alternative green energy sources and also for energy conversion.

ORCID
Djelti Radouan, https://orcid.org/0000-0002-0762-5818; **Najwa Al Bouzieh**, https://orcid.org/0000-0003-4603-9982
I. Kars Durukan, https://orcid.org/0000-0001-5697-0530; **Noureddine Amrane,** https://orcid.org/0000-0003-0555-5315

REFERENCES

[1] C. Fu, T. Zhu, Y. Liu, et al., "Band engineering of high-performance p-type FeNbSb based half-Heusler thermoelectric materials for figure of merit zT > 1," Energy Environ. Sci. **8**, 216-220 (2015). https://doi.org/10.1039/C4EE03042G
[2] G.T. Wang, and J.H. Wei, "Topological phase transition in half-Heusler compounds HfIrX (X = As, Sb, Bi)," Comput. Mater. Sci. **124**, 311 (2016). https://doi.org/10.1016/j.commatsci.2016.08.005
[3] S. Singh, S.W. D'Souza, J. Nayak, et al., "Effect of platinum substitution on the structural and magnetic properties of Ni_2MnGa ferromagnetic shape memory alloy," Phys. Rev. B Condens. Matter, **93**, 134102 (2016). https://doi.org/10.1103/PhysRevB.93.134102
[4] A. Besbes, R. Djelti, B. Bestani, and O. Akel, "First-principles study of structural, electronic, thermodynamic, and thermoelectric properties of a new ternary half-Heusler alloy PdZrGe," Chinese Journal of Physics **56**, 2926–2936 (2018). https://doi.org/10.1016/j.cjph.2018.09.027
[5] A. Roy, J.W. Bennett, K.M. Rabe, and D. Vanderbilt, "Half-heusler semiconductors as piezoelectrics," Phys. Rev. Lett. **109**, 037602 (2012). https://doi.org/10.1103/PhysRevLett.109.037602
[6] Y. Gupta, M.M. Sinha, and S.S. Verma, "Investigations of mechanical and thermoelectric properties of AlNiP novel half-Heusler alloy," Mater. Chem. Phys. **265**, 124518 (2021). https://doi.org/10.1016/j.matchemphys.2021.124518
[7] J. Nagura, T.M. Ashani, P.O. Adebambo, F. Ayedun, and G.A. Adebayo, "Thermoelectric and mechanical properties of XHfSn (X = Ni, Pd and Pt) semiconducting half-Heusler alloys: a first-principles study," Comput. Condens. Matter, **26**, e00539 (2021). https://doi.org/10.1016/j.cocom.2021.e00539
[8] Vikram, J. Kangsabanik, Enamullah, and A. Alam, "Bismuth based half-Heusler alloys with giant thermoelectric figures of merit," J. Mater. Chem. A, **5**, 6131-6139 (2017). https://doi.org/10.1039/C7TA00920H
[9] C.H. Hordequin, E. Lelievre-Berna, and J. Pierre, "Magnetization density in the half-metallic ferromagnet NiMnSb," Phys. B, **234-236**, 602-604 (1997). https://doi.org/10.1016/S0921-4526(96)01207-0
[10] J. Tobola, J. Pierre, S. Kaprzyk, R.V. Skolozdra, and M.A. Kouacou, "Crossover from semiconductor to magnetic metal in semi-Heusler phases as a function of valence electron concentration," J. Phys.: Condens. Matter, **10**, 1013 (1998). https://doi.org/10.1088/0953-8984/10/5/011
[11] K. Kaczmarska, J. Pierre, J. Beille, J. Tobola, R.V. Skolozdra, and G.A. Melnik, "Physical properties of the weak itinerant ferromagnet CoVSb and related semi-Heusler compounds," J. Magn. Magn. Mater. **187**, 210 (1998). https://doi.org/10.1016/S0304-8853(98)00125-5
[12] S. Anand, K. Xia, I.V. Hegde, U. Aydemir, V. Kocevski, T. Zhu, C. Wolverton, and G.J. Snyder, "A valence balanced rule for discovery of 18-electron half-Heuslers with defects," Energy Environ. Sci. **11**(6), 1480–1488 (2018). https://doi.org/10.1039/C8EE00306H

[13] J. Yang, H. Li, T. Wu, W. Zhang, L. Chen, and J. Yang, "Evaluation of half-Heusler compounds as thermoelectric materials based on the calculated electrical transport properties," Adv. Funct. Mater. **18**(19), 2880–2888 (2008). https://doi.org/10.1002/adfm.200701369
[14] K. Bartholomé, B. Balke, D. Zuckermann, M. Köhne, M. Müller, K. Tarantik, and J. König, "Thermoelectric modules based on half-Heusler materials produced in large quantities," J. Electronic Mater. **43**(6), 1775–1781 (2014). https://doi.org/10.1007/s11664-013-2863-x
[15] O.M. Abid, S. Menouer, A. Yakoubi, H. Khachai, S.B. Omran, G. Murtaza, D. Prakash, et al., "Structural, electronic, elastic, thermoelectric and thermodynamic properties of the NbMSb half heusler (M=Fe, Ru, Os) compounds with first principle calculations," Superlattices Microstruct. **93**, 171–185 (2016). https://doi.org/10.1016/j.spmi.2016.01.001
[16] K. Bencherif, A. Yakoubi, N. Della, O.M. Abid, H. Khachai, R. Ahmed, R. Khenata, et al., "First principles investigation of the elastic, optoelectronic and thermal properties of XRuSb:(X= V, Nb, Ta) semi-Heusler compounds using the mBJ exchange potential," J. Electron. Mater. **45**, 3479–3490 (2016). https://doi.org/10.1007/s11664-016-4488-3
[17] P.K. Kamlesh, R. Agrawal, U. Rani, and A.S. Verma, "Comprehensive ab-initio calculations of AlNiX (X = P, As and Sb) half-Heusler compounds: Stabilities and applications as green energy resources," Materials Chemistry and Physics, **275**, 125233 (2022). https://doi.org/10.1016/j.matchemphys.2021.125233
[18] Y. Wang, J. Li, J. Wang, F. He, X. Xu, Y. Liu, and F. Yin, "Prediction of NbXGe (X = Rh, Ir) half‑Heusler semiconducting compounds with promising thermoelectric property using 18‑electron rule," Applied Physics A, **128**, 44 (2022). https://doi.org/10.1007/s00339-021-05193-2
[19] D.M. Hoat, "Electronic structure and thermoelectric properties of Ta-based half-Heusler compounds with 18 valence electrons," Computational Materials Science, **159**, 470–477 (2019). https://doi.org/10.1016/j.commatsci.2018.12.039
[20] J. Wei, and G. Wang, "Thermoelectric and optical properties of half-Heusler compound TaCoSn: A first-principle study," Journal of Alloys and Compounds, **757**, 118-123 (2018). https://doi.org/10.1016/j.jallcom.2018.05.037
[21] W. Silpawilawan, Sora-at Tanuslip, Y. Ohishi, H. Muta, and K. Kurosaki, "Enhancement of thermoelectric figure of merit of p-type $Nb_{0.9}Ti_{0.1}FeSb$ half-Heusler compound by nanostructuring," Phys. status solidi a, **217**(23), 2000419 (2020). https://doi.org/10.1002/pssa.202000419
[22] P. Blaha, et al., WIEN2K, in: *An Augmented Plane Wave+ Local Orbitals Program for Calculating Crystal Propert*ies, edited by K. Schwarz, (Vienna University of Technology, Austria, 2001).
[23] P. Hohenberg, and W. Kohn, "Inhomogeneous Electron Gas," Phys. Rev. **136**(3B), B864 (1964). https://doi.org/10.1103/PhysRev.136.B864
[24] D. Singh, *Planewaves, Pseudopotentials and the LAPW Method*, (Kluwer Academic Publishers, Boston, Dortrecht, London, 1994).
[25] J.P. Perdew, K. Burke, and M. Ernzerhof, "Generalized gradient approximation made simple," Phys. Rev. Lett. **77**(18), 3865 (1996). https://doi.org/10.1103/PhysRevLett.77.3865
[26] Z. Wu, and R.E. Cohen, "More accurate generalized gradient approximation for solids," Phys. Rev. B, **73**, 235116 (2006). https://doi.org/10.1103/PhysRevB.73.235116
[27] F. Tran, and P. Blaha, "Accurate Band Gaps of Semiconductors and Insulators with a Semilocal Exchange-Correlation Potential," J. Phys. Rev. Lett. **102**, 226401 (2009). https://doi.org/10.1103/PhysRevLett.102.226401
[28] H.J. Monkhorst, and J.D. Pack, "Special points for Brillouin-zone integrations," Phys. Rev. B, **13**, 5188 (1976). https://doi.org/10.1103/PhysRevB.13.5188
[29] P. Allen, "Boltzmann Theory and Resistivity of Metals," in: *Kluwer International Series in Engineering and Computer Science*, (1996). pp. 219–250. https://doi.org/10.1007/978-1-4613-0461-6_17
[30] G.K. Madsen, D.J. Singh, "BoltzTraP. A code for calculating band-structure dependent quantities," Comput. Phys. Commun. **175**(1), 67-71 (2006). https://doi.org/10.1016/j.cpc.2006.03.007
[31] S. Adachi, *Properties of Semiconductor Alloys: Group-IV, III-V and II-VI Semiconductors*, (John Wiley & Sons, 2009). https://doi.org/10.1002/9780470744383
[32] J. Sun, H.T. Wang, and N.B. Ming, "Optical properties of heterodiamond B_2CN using first-principles calculations," Appl. Phys. Lett. **84**, 4544 (2004). https://doi.org/10.1063/1.1758781
[33] J.M. Hu, S.P. Huang, Z. Xie, H. Hu, and W.D. Cheng, "First-principles study of the elastic and optical properties of the pseudocubic Si_3As_4, Ge_3As_4 and Sn_3As_4," J. Phys.: Condens. Matter, **19**, 496215 (2007). https://doi.org/10.1088/0953-8984/19/49/496215
[34] K. Momma, and F. Izumi, "VESTA 3 for three-dimensional visualization of crystal, volumetric and morphology data," J. Appl. Crystallogr. **44**, 1272-1276 (2011). https://doi.org/10.1107/S0021889811038970
[35] T. Graf, C. Felser, and S. Parkin, "Simple rules for the understanding of Heusler compounds," Prog. Solid State Chem. **39**, 1–50 (2011). https://doi.org/10.1016/j.progsolidstchem.2011.02.001
[36] P.O. Adebambo, R.O. Agbaoye, A.A. Musari, B.I. Adetunji, and G.A. Adebayo, "Band structure, thermoelectric properties, effective mass and electronic fitness function of two newly discovered 18 valence electrons stable half-Heusler TaX(X=Co,Ir)Sn semiconductors: A density functional theory approach," Solid State Sciences, **100**, 106096 (2020). https://doi.org/10.1016/j.solidstatesciences.2019.106096
[37] C. Coban, Y.O. Ciftci, and K. Colakoglu, "Structural, electronic, elastic, optical, and vibrational properties of HfXSb (X = Co, Rh, Ru) half-Heusler compounds: an ab initio study," Indian J. Phys. **90**(11), 1233–1241 (2016). https://doi.org/10.1007/s12648-016-0873-2
[38] A. Amudhavalli, R. Rajeswarapalanichamy, and K. Iyakutti, "Half-metallic ferromagnetism in Ni based half Heusler alloys," Comput. Mater. Sci. **148**, 87–103 (2018). https://doi.org/10.1016/j.commatsci.2018.02.026
[39] G.K. Gueorguiev, J. Neidhardt, S. Stafström, and L. Hultman, "First-principles calculations on the role of CN precursors for the formation of fullerene-like carbon nitride," Chem. Phys. Lett. **401**, 288 (2005). https://doi.org/10.1016/j.cplett.2004.11.060
[40] A. Togo, and I. Tanaka, "First principles phonon calculations in materials science," Scripta Mater. **108**, 1–5 (2015). https://doi.org/10.1016/j.scriptamat.2015.07.021
[41] M. Hong, Y. Wang, T. Feng, t al., "Strong Phonon–Phonon Interactions Securing Extraordinary Thermoelectric $Ge_{1-x}Sb_xTe$ with Zn-Alloying-Induced Band Alignment," J. Am. Chem. Soc. **141**(4), 1742–1748 (2019). https://doi.org/10.1021/jacs.8b12624

[42] I. Galanakis, P. Mavropoulos, and P.H. Dederichs, "Electronic structure and Slater–Pauling behaviour in half-metallic Heusler alloys calculated from first principles," J. Phys. D. Appl. Phys. **39**, 765–775 (2006). https://doi.org/10.1088/0022-3727/39/5/S01
[43] I.K.Durukan, and Y.O. Ciftci, "First-principles calculations of vibrational and optical properties of half- Heusler NaScSi," Indian J. Phys. **95**(11), 2303 (2020). https://doi.org/10.1007/s12648-020-01887-0
[44] J.K. Satyam, and S.M. Saini, "Narrow gap electronic structure and thermoelectric performance of p-type ErMSb (M = Ni, Pd) half Heusler compounds," Physica B, **631**, 413709 (2022). https://doi.org/10.1016/j.physb.2022.413709
[45] J. Hornstra, and W. Bartels, "Determination of the lattice constant of epitaxial layers of III-V compounds," J. Cryst. Growth, **44**, 513–517 (1978). https://doi.org/10.1016/0022-0248(78)90292-0
[46] S. Wang, and H. Ye, "First-principles study on elastic properties and phase stability of III–V compounds," Phys. Status Solidi, **240**, 45 (2003). https://doi.org/10.1002/pssb.200301861
[47] M. Born, and K. Huang, *Dynamics Theory of Crystal Lattices*, (Oxford University Press, 1954).
[48] A. Iyigor, S. Al, and N. Arikan, "Density functional theory investigation on structural, mechanical, electronic and vibrational properties of Heusler alloys $AlXIr_2$ (X = Co, Cr, Cu, Fe and Zn)," Chemical Physics Letters, **806**, 140052 (2022). https://doi.org/10.1016/j.cplett.2022.140052
[49] D. Kalita, M. Ram, N. Limbu, R. Kalita, and A. Saxena, "Prediction of some physical properties in new half Heusler alloy NbAgSi," Journal of Solid State Chemistry, **310**, 122999 (2022). https://doi.org/10.1016/j.jssc.2022.122999
[50] J.-J. Shi, T. Song, P.-T. Qi, X.-Y. Wang, Z.-J. Liu, and X.-W. Sun, "Structural stabilities and half-metallicity properties of the OsTiVIn and OsZrVIn quaternary Heusler alloys under high pressure," Journal of Magnetism and Magnetic Materials, **566**, 170316 (2023). https://doi.org/10.1016/j.jmmm.2022.170316
[51] J. Haines, J.M. Leger, and G. Bocquillon, "Synthesis and Design of Superhard Materials," Annu. Rev. Mater. Res. **31**, 1 (2001). https://doi.org/10.1146/annurev.matsci.31.1.1
[52] S. Pugh, "XCII. Relations between the elastic moduli and the plastic properties of polycrystalline pure metals," London, Edinburgh, and Dublin philosophical magazine and journal of science, **45**, 823 (1954). https://doi.org/10.1080/14786440808520496
[53] S. Ahmad, S.D. Mahanti, K. Hoang, and M.G. Kanatzidis, "Ab initio studies of the electronic structure of defects in PbTe," Phys. Rev. B, **74**, 155205 (2006). https://doi.org/10.1103/PhysRevB.74.155205
[54] V. Kumar, and D.R. Roy, "Structure, bonding, stability, electronic, thermodynamic and thermoelectric properties of six different phases of indium nitride," J. Mater. Sci. **53**, 8302–8313 (2018). https://doi.org/10.1007/s10853-018-2176-9
[55] A.H. Reshak, "Thermoelectric properties of fully hydrogenated graphene: semi-classical Boltzmann theory," J. Appl. Phys. **117**, 225104 (2015). https://doi.org/10.1063/1.4922426
[56] A.H. Reshak, S.A. Khan, and S. Auluck, "Thermoelectric properties of a single graphene sheet and its derivatives," J. Mater. Chem. C, **2**, 2346–2352 (2014). https://doi.org/10.1039/C3TC32260B
[57] J.A. Abraham, R. Sharma, S. Ahmad, and A. Dey, "DFT investigation on the electronic, optical and thermoelectric properties of novel half-Heusler compounds ScAuX (X= Si, Ge, Sn, Pb) for energy harvesting technologies," Eur. Phys. J. Plus, **136**, 109 (2021). https://doi.org/10.1140/epjp/s13360-021-02021-7
[58] S. Chibani, O. Arbouche, M. Zemouli, K. Amara, Y. Benallou, Y. Azzaz, B. Belgoumene, et al., "Ab Initio Prediction of the Structural, Electronic, Elastic, and Thermoelectric Properties of Half-Heusler Ternary Compounds TiIrX (X = As and Sb)," Journal of electronic materials, **47**, 196-204 (2018). https://doi.org/10.1007/s11664-017-5761-9
[59] M.S. Dresselhaus, *Optical properties of solids*, (New York, Academic Press, 1966).
[60] G. Marius, *The Physics of Semiconductors: Kramers-kronig Relations*, (Springer, Berlin Heidelberg, 2010). pp. 775–776. https://doi.org/10.1007/978-3-642-13884-3_26
[61] C. Ambrosch-Draxl, and J.O. Sofo, "Linear optical properties of solids within the full potential linearized augmented planewave method," Comput. Phys. Commun. **175**, 1–14 (2006). https://doi.org/10.1016/j.cpc.2006.03.005
[62] M. Irfan, M.A. Kamran, S. Azam, M.W. Iqbal, T. Alharbi, A. Majid, S.B. Omran, et al., "Electronic structure and optical properties of TaNO: an ab initio study," J. Mol. Graph. Model. **92**, 296–302 (2019). https://doi.org/10.1016/j.jmgm.2019.08.006
[63] D.R. Penn, "Wave-Number-Dependent Dielectric Function of Semiconductors," Phys. Rev. **128**, 2093–2097 (1962). https://doi.org/10.1103/PhysRev.128.2093
[64] M. Gajdoš, K. Hummer, G. Kresse, and J. Furthmüller, "Linear optical properties in the projector-augmented wave methodology," Phys. Rev. B, **73**, 045112 (2006). https://doi.org/10.1103/PhysRevB.73.045112
[65] A. Azouaoui, A. Hourmatallah, N. Benzakour, and K. Bouslykhane, "First-principles study of optoelectronic and thermoelectric properties of LiCaX (X=N, P and As) half-Heusler semiconductors," Journal of Solid State Chemistry, **310**, 123020 (2022). https://doi.org/10.1016/j.jssc.2022.123020
[66] F. Benzoudji, O.M. Abid, T. Seddik, A. Yakoubi, R. Khenata, H. Meradji, G. Uğur, et al., "Insight into the structural, elastic, electronic, thermoelectric, thermodynamic and optical properties of MRhSb (M = Ti, Zr, Hf) half-Heuslers from ab initio calculations," Chinese Journal of Physics, 59, 434-448 (2019). https://doi.org/10.1016/j.cjph.2019.04.009
[67] P.K. Kamlesh, R. Gautam, S. Kumari, and A.S. Verma, "Investigation of inherent properties of XScZ (X = Li, Na, K; Z = C, Si, Ge) half-Heusler compounds: Appropriate for photovoltaic and thermoelectric applications," Physica B, **615**, 412536 (2021). https://doi.org/10.1016/j.physb.2020.412536
[68] A. Besbes, R. Djelti, and I.K. Durukan, "Study of structural, electronic, elastic, optical and thermoelectric properties of half‑Heusler compound RbScSn: A TB‑mBJ DFT study," Optical and Quantum Electronics, **54**, 372 (2022). https://doi.org/10.1007/s11082-022-03780-y
[69] R. Djelti, A. Besbes, and B. Bestani, "Investigation of electronic, optical, and thermoelectric properties of new d^0 half‑metallic half‑Heusler alloys SiLiX (X = Ca and Sr)," Emergent Materials, **5**, 1097–1108 (2022). https://doi.org/10.1007/s42247-021-00256-9
[70] D. Poelman, and P.F. Smet, "Methods for the determination of the optical constants of thin films from single transmission measurements: a critical review," J. Phys. D Appl. Phys. **36**, 1850 (2003). https://doi.org/10.1088/0022-3727/36/15/316

ДОСЛІДЖЕННЯ ЕЛЕКТРОННИХ, ПРУЖНИХ, ТЕРМОЕЛЕКТРИЧНИХ ТА ОПТИЧНИХ ВЛАСТИВОСТЕЙ НОВИХ НАПІВГЕЙСЛЕРОВИХ XRhZ (X = V, Nb ТА Z = Si, Ge) НАПІВПРОВІДНИКІВ МЕТОДОМ DFT

Сід Ахмед Бендехіба[a], Бесбес Анісса[a], Джелті Радуан[a], Найва Аль Бузіє[b], І. Карс Дурукан[c]
Нуреддін Амране[b]
[a] Лабораторія технологій і властивостей твердих тіл, Університет Мостаганем (UMAB) – Алжир
[b] Фізичний факультет, Науковий коледж, Університет Об'єднаних Арабських Еміратів (UAEU), 15551, Аль-Айн, ОАЕ
[c] Кафедра фізики, Факультет природничих наук, Університет Газі, 06500 Анкара, Туреччина

Теорія функціонала густини була використана для дослідження фізичних властивостей нових напівгейслерових сплавів XRhZ (X = V, Nb і Z = Si, Ge). Обмінно-кореляційні ефекти обробляли потенціалом TB-mBJ. Чотири досліджувані сполуки є немагнітними напівпровідниками з непрямою забороненою зоною. Ентальпія утворення, енергія когезії та фононні зонні структури показали, що ці напівпровідники є структурно та динамічно стабільними. Пружним дослідженням було передбачено, що сполуки XRhZ (X = V, Nb і Z = Si, Ge) мають стабільні механічні властивості, вони мають анізотропний характер і виявляють пластичну природу з відношенням B/G >1,75. Оптичні результати демонструють цікавий фотокаталітичний потенціал для напівпровідників NbRhSi та NbRhGe, вони демонструють високий коефіцієнт поглинання у видимій області, який становить близько 112,104 $см^{-1}$. Для енергій понад 10 еВ (УФ-домен) показник заломлення менше одиниці. Термоелектричні результати підтвердили, що сполуки XRhZ (X=V, Nb і Z=Si, Ge) дуже привабливі для термоелектричних пристроїв, що працюють у широкому діапазоні температур, включаючи температуру навколишнього середовища.

Ключові слова: *напівгейслерові сплави; напівпровідник; еластичні властивості; коефіцієнт Зеєбека; фактор заслуг; коефіцієнт поглинання; відбивна здатність*